ACS SENSORS

pubs.acs.org/acssensors

Article

Protein-Induced Fluorescence Enhancement and Quenching in a Homogeneous DNA-Based Assay for Rapid Detection of Small-Molecule Drugs in Human Plasma

Line D. F. Nielsen,[‡] Malthe Hansen-Bruhn,[‡] Minke A. D. Nijenhuis, and Kurt V. Gothelf*

Cite This: *ACS Sens.* 2022, 7, 856−865

Read Online

ACCESS | Metrics & More | Article Recommendations | Supporting Information

ABSTRACT: Homogeneous assays for determining the concentration of small molecules in biological fluids are of importance for monitoring blood levels of critical drugs in patients. We have developed a strand displacement competition assay for the drugs dabigatran, methotrexate, and linezolid, which allows detection and determination of the concentration of the drugs in plasma; however, a surprising kinetic behavior of the assay was observed with an initial rapid change in apparent FRET values. We found that protein-induced fluorescent enhancement or quenching (PIFE/Q) caused the initial change in fluorescence within the first minute after addition of protein, which could be exploited to construct assays for concentration determination within minutes in the low nanomolar range in plasma. A kinetic model for the assay was established, and when taking the new finding into account, the *in silico* simulations were in good agreement with the experimentally observed results. Utilizing these findings, a simpler assay was constructed for detection of dabigatran, which allowed for detection within minutes without any time dependencies.

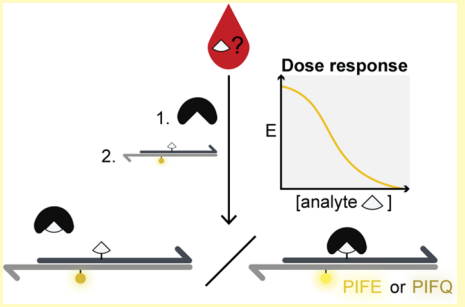

KEYWORDS: *homogeneous assay, point of care, small-molecule detection, immunoassay, quantification, DNA biosensor, PIFE, PIFQ*

As healthcare services become increasingly patient-centered, there is a growing demand for inexpensive methods that allow for quick quantification of small molecules.[1] In response to this demand, point-of-care (POC) testing has become increasingly present over the past decade. POC testing offers advantages over central laboratory testing, such as decreased turn-around time and reduced handling complexity.[1−3] Furthermore, fast-readout POC tests for determining small-molecule drug levels have vast potential for application in emergency settings, where the accurate detection and quantification of specific drugs underlie life-saving decisions. Finally, POC measurements enable patients to track and optimize the dosage of their drug therapeutics, thereby reducing side effects and potentially improving therapeutic efficacy.[4,5]

The identification and rapid quantification of small-molecule analytes in complex biological solutions are challenging. Most often, it is performed by liquid chromatography in combination with mass spectrometry techniques.[6−8] Alternative techniques for small-molecule analyte detection include enzyme-linked immunosorbent assay (ELISA);[9] although this heterogeneous detection method is applied successfully for identification of small molecules, it is often less suitable for rapid quantification.[10] Other types of heterogeneous assays for small-molecule quantification have been reported.[11−13] Homogeneous assays offer several advantages over heterogeneous assays such as ELISA, as there is no need for immobilization and washing steps, thus decreasing the turnaround time. Furthermore, they are more suitable for quantification of the analyte because there is no dependency on the quantity of immobilized species and on optical surface effects.[10,14] Homogeneous assays often employ aptamers,[15,16] DNA-binding proteins,[17,18] semisynthetic sensor proteins,[19,20] or antibodies including competitive antibody-based assays[21−25] where the readout is often based on the fluorescence or Förster resonance energy transfer (FRET). Quenchbodies offer another approach for measuring small-molecule protein interactions in solution, where the quenching of a dye linked close to the binding site of the protein is decreased upon analyte binding.[26,27] Protein-induced fluorescence enhancement (PIFE) is a related approach where a dye is linked to a protein-interacting molecule, and upon protein binding, the protein enhances the fluorescence of the dye.[28−30] PIFE has been extensively used for single-molecule fluorescence studies, in particular for DNA-binding proteins, but PIFE has also been used to study small molecule−protein interactions.[31−33]

Received: December 15, 2021
Accepted: February 18, 2022
Published: March 3, 2022

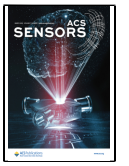

Recently, protein-induced fluorescent quenching (PIFQ) has been reported, where quenching is observed when a protein binds in proximity to a fluorophore (exhibiting the opposite effect of PIFE).[33]

We have previously reported on a homogeneous assay for overnight to 30 min detection of small molecule−protein interactions, which utilizes a strand displacement competition (SDC) system.[21,34] The mode of action of the SDC assay has previously been thought to be based on destabilization of a DNA duplex by binding of a protein to a small-molecule ligand on the DNA strand. Herein, we report on the finding of a surprising kinetic behavior of the SDC assays for detection of dabigatran (DAB), methotrexate (MTX), linezolid (LIN), and apixaban (APX). We present how the kinetic profile of the known SDC assay is dominated by protein-induced fluorescence enhancement or quenching rather than destabilization of the DNA duplex, and based on *in silico* simulations, a new mode of action of the SDC assay was determined. By exploiting this behavior, assays for quantification of the clinically relevant drugs DAB, MTX, and LIN in the low nanomolar range were constructed with a detection time of a few minutes (min) in human plasma, making these highly suitable for POC testing.

EXPERIMENTAL SECTION

General. All oligonucleotides were synthesized in-house by automated phosphoramidite oligonucleotide synthesis on a MerMade-12 RNA/DNA synthesizer using standard or modified phosphoramidites. All DNA strands were purified by reverse-phase HPLC, before utilization in an experiment, on a Hewlett Packard Agilent 1100 Series using Phenomenex Clarity 3u Oligo-RP 50 × 4.6 mm columns. Oligonucleotide concentrations were determined on a Thermo Fisher Scientific ND-1000 NanoDrop spectrophotometer. The commercially available 5-aminoallyl-dU phosphoramidite was purchased from Berry & Associates. All reagents were commercially available and bought from Sigma-Aldrich unless stated otherwise. The commercially available Amino C6 dT was purchased from Link Technologies. The Alexa dyes (Alexa555 and Alexa647) were purchased as NHS (*N*-hydroxysuccinimide) esters from Thermo Fisher Scientific. DAB was purchased from Cayman Chemical Company, the LIN amine analogue ((*S*)-5-(aminomethyl)-3-(3-fluoro-4-morpholinophenyl)oxazolidine-2-one) was purchased from Matrix Scientific, and the APX acid analogue (1-(4-methoxyphenyl)-7-oxo-6-(4-(2-oxopiperidin-1-yl)phenyl)-4,5,6,7-tetrahydro-1H-pyrazolo[3,4-*c*]pyridine-3-carboxylic acid) was purchased from Acesys Pharmatech. MTX, LIN, and APX antibodies (aMTX, aLin, and aAPX, respectively) were supplied as monoclonal antibodies by BioPorto Diagnostics A/S, while the anti-DAB fab fragment (aDab) was bought as the antidote (Idarucizumab) from Boehringer Ingelheim. All reagents were used without further purification.

Fluorescence measurements were either performed in a quartz cuvette using a scanning spectrofluorometer (FluoroMax 4 HORIBA Scientific) or in 96-well plates (COSTAR) using a plate reader (CLARIOstar, BMG Labtech). For full spectral scans on the spectrofluorometer, excitation was performed at 550 nm and emission was measured from 560 to 700 nm with an integration time of 0.09 s and 1 nm wavelength interval. For single-point measurements, excitation was performed at either 540 nm (spectrofluorometer) or 522 nm (plate reader), with emissions measured at 567 and 667 nm. FRET was calculated, taking spectral leaking into account, by $\mathrm{FRET} = \frac{F_A - 0.0815 \times F_D}{F_A + (1 - 0.0815) \times F_D}$ where F_D is emission from the donor fluorophore (Alexa555) at 567 nm and F_A is emission from the acceptor fluorophore (Alexa647) at 667 nm. FRET change (ΔFRET) and apparent FRET change (ΔaFRET) were calculated as the percentage change of (a)FRET relative to a zero-point reference, being the ABS strands pre-equilibrated in solution. All error bars are standard deviations based on triplicates.

DNA Sequences. The DNA sequences were adopted from our previous study with new ligands on the B strand.[21,34] See Tables S1 and S2 in the Supporting Information for details.

DNA-DAB and DNA-APX Conjugation. To a mixture of amine-modified DNA (10 μL, 2.0 mM), DAB (50 μL, 7.6 mM in DMSO with 10% 0.1 M HCl) or APX acid analogue (20 μL, 10 mg/mL in DMSO), and Na_2CO_3 buffer (200 μL, 20 mM, pH 8.5) was added DMTMMCl (40 μL, 0.5 M in H_2O—freshly prepared) and incubated for 25 °C for 1.5 h. The mixture was purified by ethanol precipitation followed by RP-HPLC purification.

DNA-LIN Conjugation. To a mixture of amino-modified DNA (5 μL, 2.0 mM) in Na_2CO_3 buffer (60 μL, 20 mM, pH 8.5) was added acetonitrile (40 μL) and *bis*-NHS-ester (disuccinimidyl glutarate) (20 μL, 5 mg/mL in DMF). The reaction mixture was incubated at 25 °C for 30 min followed by ethanol precipitation. The pellet was redissolved in Na_2CO_3 buffer (50 μL, 20 mM, pH 8.5), and a solution of LIN amine (25 μL, 5 mg/mL in DMF) was added, and the mixture was incubated at 25 °C overnight. The mixture was purified by ethanol precipitation followed by RP-HPLC purification.

See Scheme S1 in the Supporting Information for preparation of the *bis*-NHS-ester disuccinimidyl glutarate.

DNA-MTX Conjugation. Based on a previously reported protocol.[35] DEAE-sepharose immobilization was employed. Briefly, a 250 μL suspension of DEAE-sepharose beads is added to a spin column and washed three times with 200 μL of DNA loading buffer (10 mM acetic acid, 0.005% Triton X-100). The column is spun dry, removing the loading buffer. DNA (5−20 nmol) in DNA loading buffer (200 μL) is added. After 10 min of incubation, the liquid is removed. MTX (10 mM, 384 μL, 3.8 μmol) in DMF is added together with 1-ethyl-3-(3-dimethylaminopropyl)carbodiimide and *N*-hydroxy succinimide (each 500 mM, 8 μL, 4 μmol) in water, resulting in a total volume of 400 μL. After overnight incubation at room temperature, the reaction mixture is removed by centrifugation. The resulting slurry is washed with 200 μL of DNA loading buffer. The product is eluted with 2 × 200 μL of elution buffer (1.5 M NaCl, 50 mM Tris−HCl, pH 8.0). The mixture was purified by ethanol precipitation followed by RP-HPLC purification.

DNA-Fluorophore Conjugation. Performed according to a previous reported protocol.[21,34] Briefly, the amine-modified DNA (25 μL, 100 μM) was mixed with Alexa555 and Alexa647 NHS ester (100 μg) dissolved in DMSO or DMF (50 μL). The resulting mixture was then added to 20 mM sodium carbonate buffer (20 mM, pH 8.5; 25 μL) and incubated overnight at rt. The mixture was purified by ethanol precipitation followed by HPLC purification.

DNA-Acetylation. To an amine-modified DNA strand (9 nmol, 90 μL MQ) were added acetic anhydride (100 mM, 10 μL) and TEA (1 μL). The reaction was incubated for 2 h at rt. The mixture was purified by ethanol precipitation followed by RP-HPLC purification.

FRET Experiments. The DNA strands A, B, and S were mixed in an equal stoichiometric ratio in 1 × TAE-Mg (12.5 mM MgCl) buffer at pH 8 and incubated for minimum 2 h. The sample with or without the target molecule was preincubated with the specific protein at rt for a selected time (e.g., 1 min). The mixture was added to the DNA strands and incubated at rt for a selected time (e.g., 30 s to 1 min). In the overnight studies, all components were mixed and incubated at rt in the dark overnight. Figures showing both kinetic traces and overnight FRET are based on two separate experiments. Overnight FRET studies are always a distinct experiment performed as described above.

For experiments in plasma, EDTA-buffered human blood from a healthy unknown donor was acquired from the local blood bank (Aarhus University hospital, Denmark). The blood was centrifuged to separate the cells from plasma at 3.000 rcf for 15 min at rt. The plasma was then spiked with small molecules and incubated with the protein, before addition to the DNA strands as described above.

Limit of Detection. The limit of detection (LOD) was calculated based on the equation given below.[36]

https://doi.org/10.1021/acssensors.1c02642
ACS Sens. 2022, 7, 856−865

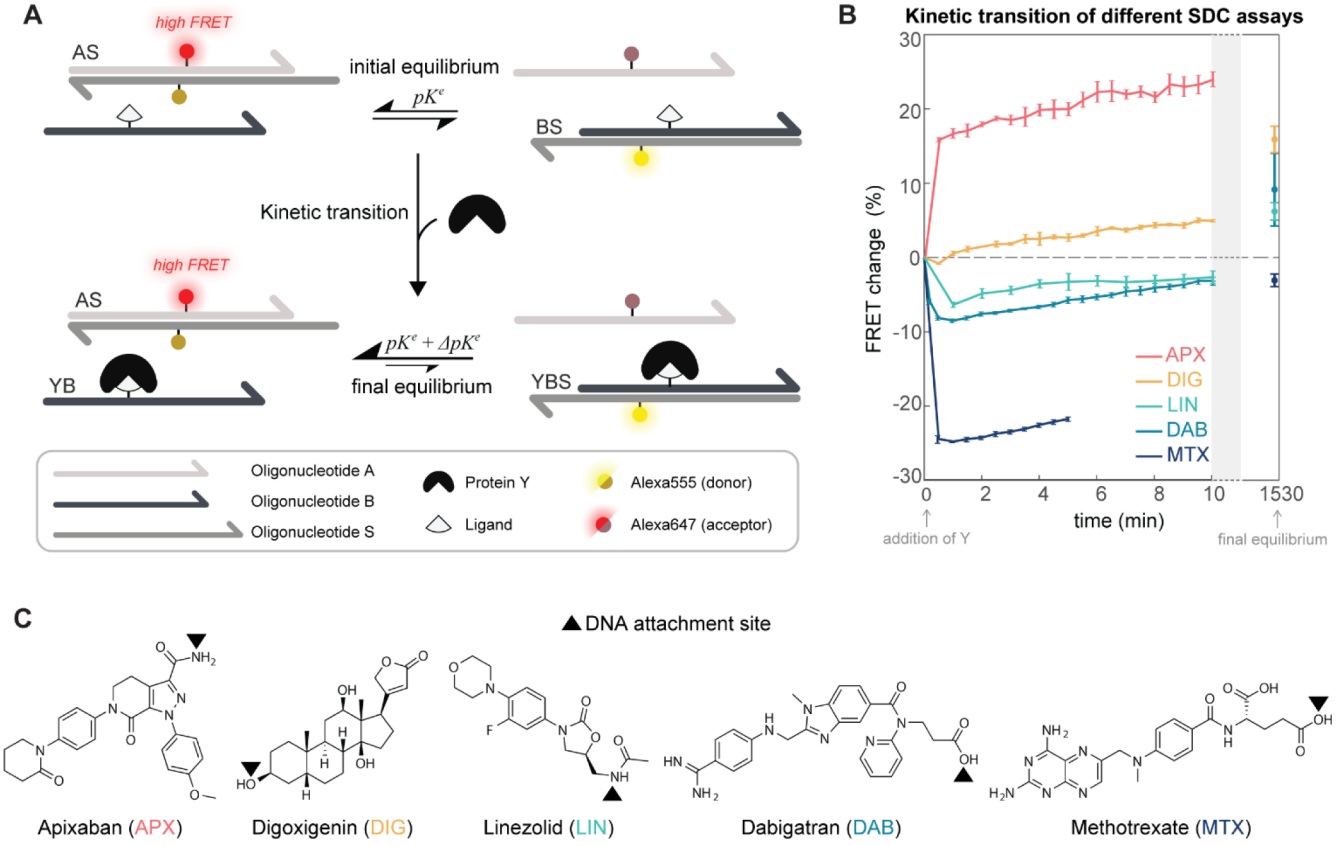

Figure 1. SDC assay. (A) Three DNA strands A, B, and S are in a dynamic equilibrium, which can be monitored by FRET readout as the S and A strands are modified with fluorophores. The B strand contains a small-molecule ligand. The addition of the biomolecular binding partner (Y) of the ligand on the B strand results in a kinetic transition, yielding an increase in FRET. (B) Change in FRET over time of the five investigated assays after addition of protein (Y); APX assay (red), digoxigenin (DIG) assay (yellow), LIN assay (light green), DAB assay (teal), and MTX assay (dark blue). (C) Structure of the small molecules investigated: APX, DIG, LIN, DAB, and MTX. The site at which these are attached to the B strand is denoted with an arrowhead.

$$\mathrm{LOD} = \frac{3 \times \sigma(\text{low concentration})}{\Delta\text{FRET change}}$$

Slopes of the linear range of the concentration curves of DAB, MTX, and LIN were used as ΔFRET change. The standard deviation from the lowest concentration in each concentration curve was used as σ. See Figures S1−S3 for graphs and calculations.

Mathematical Model. The initial competitive strand displacement equilibrium was characterized as a steady-state system based on the conservation of mass. In order to mechanistically evaluate the kinetic transition upon protein addition and eventual final equilibrium, a kinetic model based on the laws of mass action was used. The model takes as input (1) the DNA species concentrations calculated with the steady-state characterization, (2) the concentration of protein added, and (3) five parameter values. The latter are the strand displacement equilibrium constant (pK^e), its change upon equilibrium shift (ΔpK^e), one rate of strand displacement (k^B), and finally the dissociation and rate constants describing the protein's affinity toward its ligand (K^d and k^{on}). The model describes the concentrations of each species changing over time until they settle in a new equilibrium, using a system of eight coupled ordinary differential equations (ODEs). Certain parameters are quantifiably restricted in order to model specific hypothesized mechanisms, for example, $\Delta pK^e > 0$ for protein-induced destabilization of BS. Finally, eq 4 describes the conversion from modeled concentrations to simulated ΔaFRET, which may require the PIFE/Q parameter r. The full derivation and ODE system are found in the Supporting Information, 'Model Derivation'. The calibration and validation methods for comparison between simulated ΔaFRET and measured ΔaFRET are described in the Supporting Information "Model Fitting".

RESULTS AND DISCUSSION

In the SDC system, two DNA strands A and B dynamically compete for the binding of a third strand S through toehold-mediated strand displacement (Figure 1A). The equilibrium between the three strands depends on the relative stability of the resulting two duplexes (AS and BS): if one duplex is destabilized, the equilibrium will shift to favor the other. This competitive equilibrium is quantified by the equilibrium constant pK^e (eq 1). Furthermore, its change (ΔpK^e) may be monitored through a fluorescent readout based on FRET. Specifically, the hybridization of the S and A strands brings the fluorescent labels in close proximity, resulting in increased FRET. The final FRET readout is a ratiometric representation of the AS and BS duplexes, thereby enabling direct quantification of these species.

$$pK^e = \log \frac{[AS][B]}{[A][BS]} \quad (1)$$

$$\mathrm{FRET} = \frac{F_A}{F_A + F_D} \quad (2)$$

where [A] and [B] are the concentrations of the strands competing for the S-strand, [AS] and [BS] are the concentrations of their respective duplexes, and F_A and F_D are, respectively, the acceptor and donor emission intensity. To employ the SDC system in an assay for molecule−protein

https://doi.org/10.1021/acssensors.1c02642
ACS Sens. 2022, 7, 856−865

interactions, the B strand is conjugated to a small molecule of interest via a base in one of the nucleotides. This modification has little impact on the BS duplex stability, presumably because it is relatively small.[21] However, once a protein (Y) binds the small molecule as its ligand, the stability of the BS duplex may be significantly affected. Specifically, the mode of action of the SDC-based assay was hypothesized to be as follows: the binding of a bulky protein Y to the B-conjugate creates steric repulsion that explicitly destabilizes the BS duplex (Figure 1A). Consequently, upon addition of the protein to the SDC system, the competitive equilibrium shifts in favor of hybridization between A and S. Since AS is more dominant in the final equilibrium, the final FRET signal is increased compared to FRET measured at the initial state. If the protein is preincubated with a sample containing an unknown amount of free small-molecule ligand and thereby the binding site is partly blocked, its addition to the SDC system is proportionally less effective in causing the anticipated equilibrium shift ΔpK^e. The final FRET readout can thereby also be used to quantify an unknown concentration of ligand in a sample of interest.

Kinetic Behaviors of SDC Assays. The hypothesized mechanism was in excellent agreement with the observed behavior of the first SDC-based assay, which studied the interaction between the ligand digoxigenin (DIG),[21,34] a drug used to treat cardiac arrhythmia,[37] and the anti-DIG antibody (Figure 1B, yellow). A slow increase in the FRET signal was observed after protein addition, consistent with the protein-induced destabilization of BS. The DIG assay fully settled into its final equilibrium after overnight incubation, although it should be noted that a fully settled equilibrium is not necessary for real-life application of the assay. In comparison, no significant increase was observed when the protein had been preincubated with an excess of free ligand.[34] The readout obtained from the SDC assay allows for quantification of small molecules, such as digoxigenin and folate in plasma, at therapeutically relevant ranges, with its fastest readout time being 30 min.[21,34]

Surprisingly, very different kinetics were observed for some other protein/small molecule pairs (Figure 1B).

Looking for additional applications of the SDC assay, we were interested in monitoring of blood concentrations of a class of medication called direct oral anticoagulants (DOACs). The drug DAB belongs to this class and is a direct thrombin inhibitor,[38,39] which is clinically used as an anticoagulant to prevent blood clots. For construction of the SDC assay, DAB was conjugated to the B strand and anti-DAB Fab was used as the protein. When the anti-DAB protein was added to the assay, however, a rapid decrease in FRET over 1−2 min was observed, followed by the anticipated slow increase over time (Figure 1B, teal).

Prompted by this unexpected finding, we decided to test the SDC system with three more targets: LIN, an antibiotic used in the treatment of Gram-positive bacteria,[40] MTX, an immunosuppressant often used as a chemotherapeutic agent,[41] and APX, which is a Factor Xa inhibitor anticoagulant also belonging to the DOACs.[42] Custom-raised monoclonal antibodies against LIN, MTX, and APX were used as biomolecular binding partners. The LIN assay displayed a similar kinetic profile as the DAB assay (Figure 1B, light green). The MTX assay displayed an even more pronounced initial decrease than the DAB assay, followed by the similar gradual increase (Figure 1B, dark blue). The FRET measured in the final equilibrium state was lower than in that of the initial state; this was an especially peculiar observation as it seems to imply that the BS duplex—which is supposedly destabilized by the protein Y—is more dominant in the final equilibrium. Perhaps even more surprising was that the APX assay, which showed a very rapid initial *increase*, was followed again by the anticipated slow increase (Figure 1B, red). An overview of all five small molecules of interest is shown in Figure 1C. It should be noted that the FRET only changed when a B-strand was incubated with a compatible protein (Figure S4). Furthermore, any FRET changes were also fully inhibited by the presence of a compatible free ligand. The behavior thus requires binding specificity and does not result from an arbitrary protein or conjugate.

Original Mechanism of Action of the SDC Assay. In order to understand the unexpected kinetic behavior of the assay, a mechanistic model based on mass action kinetics was drawn up in order to test the hypothesized mode of action (Supporting Information "Model Derivation"). A number of assumptions are made about the SDC system, which enables the model to specifically simulate the protein-induced destabilization of the BS mechanism. The prime assumption herein is that the change in ΔpK^e must be positive, that is, protein addition must cause a shift toward a more AS-dominant state. Equation 3 converts the simulated concentration of the competing species to a predictive FRET change (ΔFRET), at a certain timepoint t (Supporting Information "Model Derivation"), which can then be compared to the experimentally observed ΔFRET.

$$\Delta\mathrm{FRET}_t = \frac{[\mathrm{AS}]_t([\mathrm{AS}]_{t=0} + [\mathrm{BS}]_{t=0})}{[\mathrm{AS}]_{t=0}([\mathrm{AS}]_t + [\mathrm{BS}]_t + [\mathrm{YBS}]_t)} \cdot 100\% \quad (3)$$

After calibration, the mechanistic model could reliably replicate the FRET change of the original DIG assay, which showed only the anticipated slow signal increase (Figure S15A). However, even with a loose interpretation of unknown parameters and uncertainties, this model was unable to simulate the fast signal decrease of the DAB assay (Figure S15B), let alone the entire behavioral variety observed over all five assays (Figure S15C). Therefore, the original hypothesis of the mechanism of the SDC assay is insufficient. Although all assays eventually show a slow signal increase consistent with protein-induced destabilization of BS, a different mechanism must dominate the assay's readout in the initial minutes of the kinetic transition.

Extended Mechanism of Action of the SDC Assay. After unsuccessful testing of several equilibrium-based hypothesized mechanisms (e.g., complexation of multiple species), we took a closer look at the raw fluorescence data forming the basis of the FRET readout. During the kinetic transition, a rather large initial change in donor intensity was observed, without a concomitant change of the acceptor fluorophore. This is inconsistent with the typical FRET measurement, in which the donor emission is inversely related to the acceptor emission. Addition of the relevant protein to the DAB or MTX assays caused a drastic increase in donor emission, while the acceptor emissions remained unchanged (Figure 2A). Thus, the observed FRET change is only an apparent FRET change (ΔaFRET), resulting from the division of the observed intensities rather than an accurate measure of the Förster energy transfer. In the BS duplex, the small-molecule ligand of the B strand is situated closely to the fluorophore of the S strand (Figure 2E). We therefore

https://doi.org/10.1021/acssensors.1c02642
ACS Sens. 2022, 7, 856−865

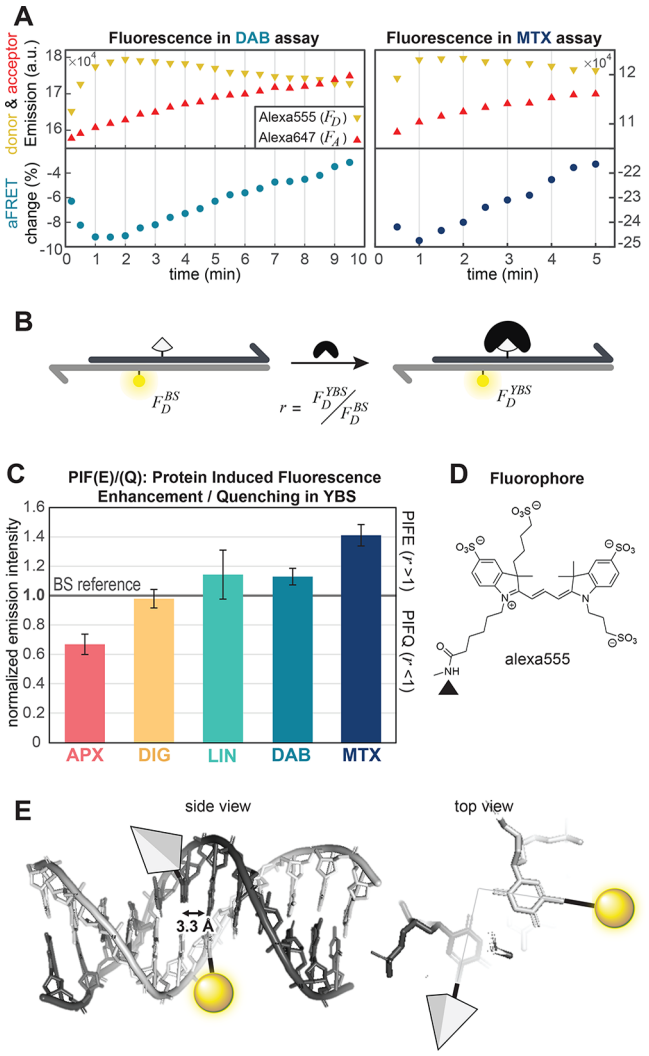

Figure 2. (A) Donor and acceptor emission and calculated aFRET values for the ABS system for DAB and MTX after addition of the respective protein. (B) Setup for evaluating the impact of the binding of the protein to the BS-strand (PIFE/Q). This impact is quantified with the r parameter, which is the unitless ratio of the respective fluorescent intensities of BS and YBS. (C) Results of the effect of protein on the BS duplexes (60 nM assay). The BS reference is the BS duplex with the acetylated B-strand (B_{ACET}). Error bars represent standard deviations. (D) Structure of the donor fluorophore, Alexa555, and the DNA attachment site (black triangle). (E) 3D rendering of the BS duplex with the fluorophore and ligand. The ligand and fluorophore are placed on adjacent t-bases, which colocalizes the species (PDB 1BNA).

hypothesized that the binding of the protein to the small-molecule ligand will influence the emission of the nearby fluorophore, either enhancing or quenching the fluorescence (PIFE or PIFQ, respectively). The effects caused by an increased local viscosity induced by the proximity of the protein may impair the fluorophore, which may result in increasing or decreasing fluorescent intensities when some of the nonirradiative excitation decay pathways are inhibited or promoted.[33]

To investigate the interaction of the protein with the fluorophore of the S-strand, we investigated the BS duplex in the absence and presence of protein (Figure 2B). In the case of DAB, LIN, and MTX, the protein caused an enhancement of the fluorescence (PIFE). For APX, addition of the protein caused a large quenching of the fluorescence (PIFQ) (Figure 2C, red). As a control, we added the various proteins to the BS duplex with the acetylated B-strand, which did not give rise to a change in the fluorescence, confirming the necessity of the specific binding of the protein to the ligand (Figure S5).

It is peculiar that some of the proteins cause an enhancement of fluorescence, while others cause quenching. Despite the photophysical model of PIFE,[30] the relationship between the protein structure and PIFE/Q largely remains a mystery. While it has been proven that different DNA sequences can explain PIFE/Q variability (e.g., due to intramolecular folding and/or guanine-induced quenching),[33] the sequences of the ABS strands were kept constant—as were the positions of the protein and dye. It has been shown that even slight changes in the molecular structure can impact the PIFE/Q effect.[43] The difference between the observed effects of our investigated proteins could potentially be caused by different amino acid composition of the parts of the proteins that are in proximity to the fluorophore.

The collective PIFE/Q effects of each individual ligand/protein pair are quantified with r, defined as the ratio between emission intensity from the protein-bound duplex (YBS) and unbound duplex (BS). The value of r is smaller than 1 if the protein has a quenching effect and vice versa for an enhancing effect.

The findings on the donor emission manipulation form the basis of a new hypothesis on the SDC assay's mechanism of action. The protein-induced destabilization of BS causing a shift in the strand displacement equilibrium is responsible for the gradual long-term signal increase observed in all assays. Additionally, the protein can induce a significant and almost immediate change in donor fluorescence when it is bound to the BS duplex. In order to test this hypothesis, we modified the mechanistic model that previously failed to replicate the experimental behavior. The only change was the introduction of the PIFE/Q parameter r into eq 3, which is used to convert the concentration of species into a FRET signal. This parameter only affects the protein-bound species YBS (eq 4).

$$\Delta\mathrm{FRET}_t = \frac{[\mathrm{AS}]_t([\mathrm{AS}]_{t=0} + [\mathrm{BS}]_{t=0})}{[\mathrm{AS}]_{t=0}([\mathrm{AS}]_t + [\mathrm{BS}]_t + r[\mathrm{YBS}]_t)} \cdot 100\% \tag{4}$$

The modified model was again fitted against all five assays simultaneously, to test whether it could explain the entire behavior variety. Both $\widehat{\Delta pK^e}$ and $\hat{r}$ are estimated uniquely for each assay because these parameters are specific to the protein/ligand pair and essential to the hypothesized mechanism. Parameters and constants that are assumed invariant between distinct systems are elaborated on in the Supporting Information "model fitting". This fit shows a remarkable agreement between simulation and experiment (Figure 3A), even under the strict interpretation of the hypothesis and significant simplification of the overall system (as explained in the Supporting Information "Model Fitting"). Furthermore, the standard error on the estimated parameter values is low, suggesting a quantitative certainty in the estimated values. Indeed, comparing the $\hat{r}$ estimates against the experimentally measured r reveals that there is no significant difference between the theoretical model values and the assay observations (Figure 3B). As expected, the LIN, DAB, and MTX assays all have an r higher than 1, indicating

https://doi.org/10.1021/acssensors.1c02642
ACS Sens. 2022, 7, 856−865

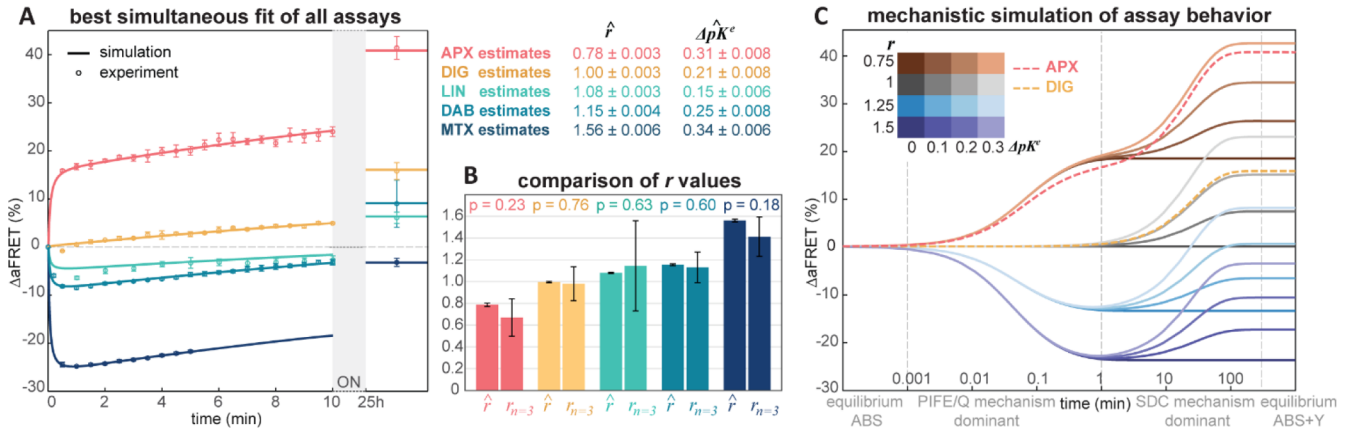

Figure 3. A) Best fit of the mechanistic model with all five assay systems simultaneously. The fit shows a good agreement between wetlab data (markers with error bars) and simulation (lines). The model incorporates both protein-induced destabilization of BS (quantified by ΔpK^e) and the PIFE/Q effect (quantified by r). The model-estimated values for these parameters are shown in boxes. The remaining constants and parameters are reported in Table S4. Error bars represent standard deviations. (B) Model-estimated $\hat{r}$ values are quantitatively comparable to experimental r values measured in triplicate. P-values shown were calculated with Welch's t-test. Note that r is a unitless ratio. Error bars represent 95% confidence intervals. (C) Predictive simulation of possible assay behaviors, depending on the extent of protein-induced destabilization (ΔpK^e, brightness gradient) and PIFE/Q (r, hue gradient). Plotting on a logarithmic timescale reveals that PIFE/Q effects dominate the assay behavior in the initial minute after protein addition. Protein-induced destabilization becomes apparent after the first minute, until the system settles in the final equilibrium. The final assay readout after a few hours is the culmination of both mechanisms. The DIG and APX traces are identical to the ones given in subfigure A and are added to ease the comparison of the natural and logarithmic timescales.

the presence of PIFE. The APX assay has an r lower than 1, indicating PIFQ. Finally, the DIG assay has an r of 1, meaning that the protein has no effect on the fluorescence emission.

The equilibrium shift ΔpK^e also varies between assays, but in all cases, it is relatively small (between 0.15 and 0.31) and never close to a full order of magnitude. Based on the estimated ranges of ΔpK^e and r, a predictive simulation of possible assay outcomes of other ligand/protein pairs was performed (Figure 3C). Plotting kinetic traces on a logarithmic timescale cleanly reveals the two-phased behavior of the SDC-based assays: in the initial minute, the PIFE/Q effects are the main drivers behind the change in the apparent FRET signal, whereas afterward, the protein-induced destabilization of BS is the dominant mechanism. This two-phased behavior is the result of the on-rate of the protein binding being several orders of magnitude greater than the rates of the strand displacement reactions. The final apparent FRET readout after a few hours is the culmination of both mechanisms. Consequently, the final FRET readout may be decreased compared to the initial signal, even as the equilibrium shifts in favor of the FRET-active species AS.

Construction of Assays for Rapid Detection of DAB, MTX, and LIN. Before realizing the true mechanism of action of the SDC assay, the rapid change in kinetics in the first few minutes caused by PIFE/Q was exploited to develop assays for rapid detection of DAB, MTX, and LIN. Here, the biomolecular binding partner Y and the free analyte were incubated first, followed by the incubation with the equilibrated DNA strands, allowing for a detection system as seen in Figure 4A.

The incubation time needed for the protein to be fully inhibited with the free analyte was investigated and found to be 1 min for DAB and LIN (Figures S6 and S7) and 30 s for MTX. Due to rapid detection time, these assays have high potential for POC applications.

For all three target molecules, PIFE is dominant in the initial minutes (Figure 4A). As the timescale for detection in these assays is all within minutes, the effect from the shift in the DNA equilibrium is negligible (Figure 3C). When the analyte is not present, the protein will bind to the B-strand, causing fluorescent enhancement of the donor fluorophore, which in turn appears as low aFRET (Figure 4A top). An increased amount of analyte in the first incubation step will occupy the protein to a larger degree, thereby resulting in less interaction of the protein with the modified B-strand.

In turn, there is less fluorescent enhancement of the donor fluorophore, resulting in a higher aFRET (Figure 4A bottom). Thus, an increase in ΔaFRET occurs with increasing analyte concentration. Modulating the concentration of the analyte allows for the construction of dose−response curves, as shown in Figure 4B−D. For DAB, dose−response curves at three different assay concentrations (1:1 ratio between Y:A:B:S at 10, 20, and 40 nM) were established, with 2 min total detection time (Figure 4B, left).

As is evident from the curve, the linear range of the assay is tunable by the assay concentration. Therefore, we hypothesize that the system can be tuned to the desired range for any application only limited by the Kd of the protein. A similar setup was built with the MTX assay with assay concentrations at 10, 20, and 40 nM (Figure 4C, left). Here, the total detection time was 1 min, consisting of 30 s incubation of protein with free analyte and 30 s of the mixture with the DNA strands. A similar dose−response curve is obtained as for DAB. Saturation of aDAB and aMTX with DAB and MTX occurs at 1:1 ratio and 1:2 ratio, respectively, presumably due to aDab having only one binding site (Fab fragment) and aMTX having two binding sites (full antibody). Both assays exhibited stable performance in the range of 5−35 °C (Figures S8 and S9).

Detection in Human Plasma. To advance the technology further toward POC applications, we investigated the ability of the assay to measure small molecules in human plasma. First, the impact of plasma on the kinetics of the DAB assay was investigated. The FRET minima were delayed by one min compared to the rate in buffer, which presumably is caused by

https://doi.org/10.1021/acssensors.1c02642
ACS Sens. 2022, 7, 856−865

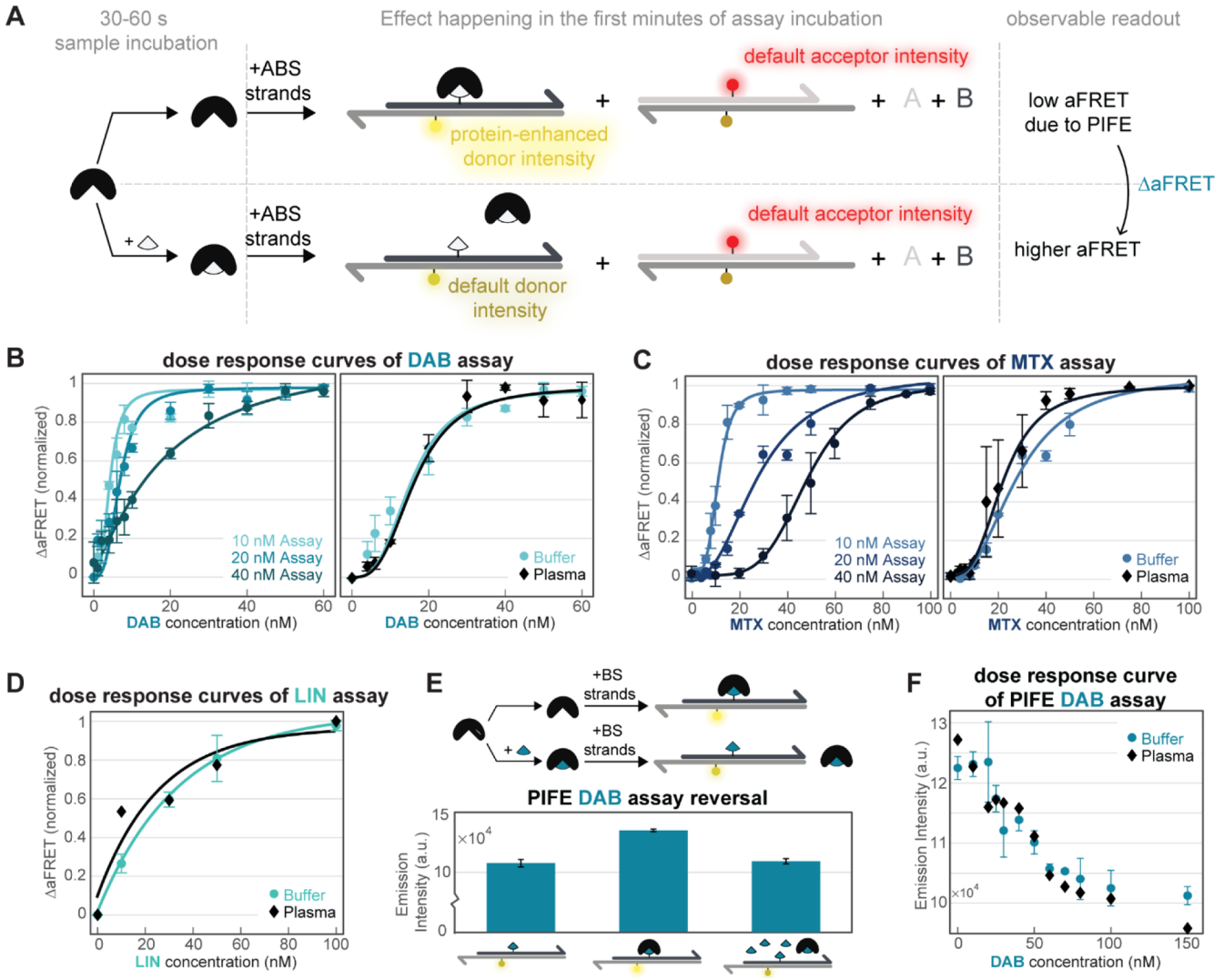

Figure 4. Setup for detection and quantification of small molecules exploiting the PIFE effect (A) Protein is mixed with the sample that contains the small molecule analyte and allowed to react (30−60 s). To the mixture are added the preequilibrated ABS strands. Within the first minute, the PIFE effect is dominant. With small molecule present, no PIFE occurs, resulting is less fluorescent enhancement and thus a higher aFRET. When no small molecule is present, fluorescent enhancement occurs, thus giving a lower aFRET. (B) Left: Employing 1 min preincubation time and 1 min interaction with the DNA strands, a dose response in the low nanomolar range can be obtained. Using three different concentrations of the DAB assay, several distinct dose−response curves can be constructed. Right: In plasma, a 1 min incubation step followed by 2 min of interaction with the DNA strands shows a similar response in 65% human plasma for detection of DAB as in buffer. (C) Left: For detection of MTX, a 30 s incubation step was employed together with a 30 s readout step, resulting in a dose−response curve in the low nanomolar range within 1 min. Similarly, three different concentrations allow for tuning of the dynamic range. Right: Detection in 65% human plasma within 1 min shows similar performance as in buffer. (D) Comparison of 20 nM LIN assay in buffer and in human plasma (88%). (E) PIFE DAB assay using only the B_{DAB} and S-strand can be constructed measuring only donor emission. The PIFE effect can be reversed by addition of excess DAB. (F) Dose−response curves in both buffer and 65% human plasma of the PIFE DAB assay. Detection time is 2 min: 1 min of incubation of the protein with the sample and a 1 min readout.

the higher viscosity of plasma (shown in Figure S10). Therefore, the total assay time in the concentration study in plasma for DAB and LIN is 3 min and 1 min of incubation with aDAB or aLIN, followed by 2 min of incubation with the DNA strands. For MTX, no change in time of the minima in FRET was observed during measurement in plasma (Figure S11); hence, a detection time of 1 min for MTX was maintained. Detection in buffer and detection in plasma are shown in Figure 4B−D for DAB, MTX, and LIN, respectively. From the data, it is evident that the systems perform similarly in buffer and plasma. The LOD was calculated to be 2.25 and 4.75 nM for DAB and MTX in plasma, respectively (Figures S1 and S2) and 8.79 nM for LIN in buffer (Figure S3). Due to the lack of studies correlating plasma concentration with thrombic and hemorrhagic complications, DAB has no reported therapeutic range.[44] The lowest concentration at which DAB is present in the blood, in patients taking a normal dose, has been determined to be above 38 nM.[44] Studies show that a plasma concentration of MTX after treatment of 0.1−10 μM within 24−72 h can be toxic.[45] An optimal therapeutic range of LIN in critically ill patients has been determined to be between 5.9 and 29.6 μM.[46] These assays are therefore capable of detecting all DAB, MTX, and LIN at subtherapeutic levels in plasma within minutes. This fast readout is highly desired for POC applications, for example, an emergency setting or for therapeutic drug monitoring.

https://doi.org/10.1021/acssensors.1c02642
ACS Sens. 2022, 7, 856−865

The cross-reactivity between the three assays was investigated, to demonstrate the selectivity of these systems. No cross-reactivity was observed between the antibodies and the three different small molecules (Figure S12).

PIFE-Based Assay for the Detection of Small Molecules. To further confirm that the change in FRET within the first few minutes is derived from a PIFE/Q effect and that this can be utilized as an assay readout, a simpler assay was constructed using only the S- and B-strand (the setup is shown in Figure 4E). By omitting the A-strand, the readout of the assay is only based on the influence of the protein on the donor fluorophore, and the signal readout is not time-dependent as is the case for the SDC assay. Using the new PIFE assay, a method consisting of 1 min of incubation with the protein and the sample, followed by 1 min of incubation of the mixture with DNA strands, provided a 2 min PIFE assay for detection of DAB. In a 60 nM setup, it is possible to reverse the PIFE effect by 1 min of incubation with DAB (Figure 4E), and the PIFE assay can detect DAB in the nanomolar range in buffer and in plasma (Figure 4F). Removing the strand displacement equilibrium from the system increased the total signal change from 8% signal change in the original SDC assay (Figure 1B, DAB) to 20% signal change in the novel assay. To the best of our knowledge, this is the first reported PIFE assay for small-molecule quantification.

CONCLUSIONS

Based on our previously reported SDC-based assay, we developed efficient assays for the detection of clinically relevant drugs such as the DOAC DAB, the immunosuppressant MTX, and the antibiotic LIN in plasma. Unexpectedly, the FRET changed rapidly in the initial minutes of sample incubation. In silico experiments elucidated that the apparent kinetic readout of the SDC assay is two-phased. On the hour-timescale of all assays, the biomolecular binding partner induced a slow signal increase through the thermodynamic destabilization of one of the competing DNA duplexes. However, the protein binding also had another effect; upon binding the DNA duplex; the nearby donor fluorophore emission is in most cases either enhanced or quenched through PIFE/Q. In such assays, the apparent FRET then responds immediately yet counterintuitively. It increases when the donor is quenched and vice versa. The first few minutes of these assays are thus dominated by a fluorescent artifact, rather than an equilibrium shift. This mode of action enabled the development of a fast-readout SDC-based assay that quantitatively detects the target analyte in less than 3 min. A simplified version of the assay, where the signal is purely generated using the PIFE/Q effect, detected nanomolar ranges of DAB in plasma. These assays show a great potential for application in POC systems as these are rapid and robust and are well-behaved in human plasma.

ASSOCIATED CONTENT

Supporting Information

The Supporting Information is available free of charge at https://pubs.acs.org/doi/10.1021/acssensors.1c02642.

DNA sequences, laboratory experiments, model derivation, model fitting, and hypothesis testing with experimental data (PDF)

AUTHOR INFORMATION

Corresponding Author

Kurt V. Gothelf − *Interdisciplinary Nanoscience Center (iNANO) and Department of Chemistry, Aarhus University, 8000 Aarhus C, Denmark;* orcid.org/0000-0003-2399-3757; Email: kvg@chem.au.dk

Authors

Line D. F. Nielsen − *Interdisciplinary Nanoscience Center (iNANO) and Department of Chemistry, Aarhus University, 8000 Aarhus C, Denmark;* Present Address: MedicQuant ApS, Universitetsbyen 14, 8000 Aarhus C, Denmark

Malthe Hansen-Bruhn − *Interdisciplinary Nanoscience Center (iNANO) and Department of Chemistry, Aarhus University, 8000 Aarhus C, Denmark;* Present Address: MedicQuant ApS, Universitetsbyen 14, 8000 Aarhus C, Denmark

Minke A. D. Nijenhuis − *Interdisciplinary Nanoscience Center (iNANO) and Department of Chemistry, Aarhus University, 8000 Aarhus C, Denmark*

Complete contact information is available at: https://pubs.acs.org/10.1021/acssensors.1c02642

Author Contributions

‡L.D.F.N. and M.H.-B. contributed equally. All authors have given approval to the final version of the article.

Notes

The authors declare no competing financial interest.

ACKNOWLEDGMENTS

We are grateful for the financial support to this work from the Innovation Fund Denmark to DETECT, to the Novo Nordic Foundation for support to Center for Multifunctional Biomolecular Drug Design (grant no. NNF17OC0028070), and to DNA Robotics, Marie Skłodowska-Curie ITN under Horizon 2020 (grant no. 765703). Some of the computing for this project was performed on the GenomeDK cluster. We would like to thank GenomeDK and Aarhus University for providing computational resources and support that contributed to these research results.

ABBREVIATIONS

APX, apixaban; aAPX, anti-apixaban antibody; DAB, dabigatran; aDAB, anti-dabigatran fab fragment; LIN, linezolid; aLIN, anti-linezolid antibody; MTX, methotrexate; aMTX, anti-methotrexate antibody; DIG, digoxin; aDIG, anti-digoxigenin antibody; rt, room temperature; FRET, Förster resonance energy transfer; ODE, ordinary differential equation; PIFE, protein-induced fluorescent enhancement; PIFQ, protein-induced fluorescent quenching; POC, point of care; SDC, strand displacement competition

REFERENCES

(1) St John, A.; Price, C. P. Existing and Emerging Technologies for Point-of-Care Testing. *Clin. Biochem. Rev.* **2014**, *35*, 155−167.

(2) Salem, M.; Chernow, B.; Burke, R.; Stacey, J.; Slogoff, M.; Sood, S. Bedside diagnostic blood testing: Its accuracy, rapidity, and utility in blood conservation. *JAMA, J. Am. Med. Assoc.* **1991**, *266*, 382−389.

(3) Larsson, A.; Greig-Pylypczuk, R.; Huisman, A. The State of Point-of-Care Testing: A European Perspective. *Upsala J. Med. Sci.* **2015**, *120*, 1−10.

(4) Touw, D. J.; Neef, C.; Thomson, A. H.; Vinks, A. A. Cost-Effectiveness of Therapeutic Drug Monitoring: A Systematic Review. *Ther. Drug Monit.* **2005**, *27*, 10−17.

(5) Luppa, P. B.; Müller, C.; Schlichtiger, A.; Schlebusch, H. Point-of-Care Testing (POCT): Current Techniques and Future Perspectives. *Trends Anal. Chem.* **2011**, *30*, 887−898.
(6) Maurer, H. H. Current Role of Liquid Chromatography-Mass Spectrometry in Clinical and Forensic Toxicology. *Anal. Bioanal. Chem.* **2007**, *388*, 1315−1325.
(7) Yang, Z.; Wang, S. Recent Development in Application of High Performance Liquid Chromatography-Tandem Mass Spectrometry in Therapeutic Drug Monitoring of Immunosuppressants. *J. Immunol. Methods* **2008**, *336*, 98−103.
(8) Dahal, U. P.; Jones, J. P.; Davis, J. A.; Rock, D. a. Small Molecule Quantification by Liquid Chromatography-Mass Spectrometry for Metabolites of Drugs and Drug Candidates. *Drug Metab. Dispos.* **2011**, *39*, 2355−2360.
(9) Lequin, R. M. Enzyme Immunoassay (EIA)/ Enzyme-Linked Immunosorbent Assay (ELISA). *Clin. Chem.* **2005**, *51*, 2415−2418.
(10) Dinis-Oliveira, R. J. Heterogeneous and Homogeneous Immunoassays for Drug Analysis. *Bioanalysis* **2014**, *6*, 2877−2896.
(11) Yan, J.; Van Smeden, L.; Merkx, M.; Zijlstra, P.; Prins, M. W. J. Continuous Small-Molecule Monitoring with a Digital Single-Particle Switch. *ACS Sens.* **2020**, *5*, 1168−1176.
(12) Daems, D.; Lu, J.; Delport, F.; Mariën, N.; Orbie, L.; Aernouts, B.; Adriaens, I.; Huybrechts, T.; Saeys, W.; Spasic, D.; Lammertyn, J. Competitive Inhibition Assay for the Detection of Progesterone in Dairy Milk Using a Fiber Optic SPR Biosensor. *Anal. Chim. Acta* **2017**, *950*, 1−6.
(13) Ruiz-Valdepeñas Montiel, V.; Sempionatto, J. R.; Vargas, E.; Bailey, E.; May, J.; Bulbarello, A.; Düsterloh, A.; Matusheski, N.; Wang, J. Decentralized Vitamin C & D Dual Biosensor Chip: Toward Personalized Immune System Support. *Biosens. Bioelectron.* **2021**, *194*, 113590.
(14) Zhang, H.; Li, F.; Dever, B.; Li, X.-F.; Le, X. C. DNA-Mediated Homogeneous Binding Assays for Nucleic Acids and Proteins. *Chem. Rev.* **2013**, *113*, 2812−2841.
(15) Sassolas, A.; Blum, L. J.; Leca-bouvier, B. D. Homogeneous Assays Using Aptamers. *Analyst* **2011**, *136*, 257−274.
(16) Nutiu, R.; Li, Y. Structure-Switching Signaling Aptamers. *J. Am. Chem. Soc.* **2003**, *125*, 4771−4778.
(17) Wang, J.; Li, T.; Guo, X.; Lu, Z. Exonuclease III Protection Assay with FRET Probe for Detecting DNA-Binding Proteins. *Nucleic Acids Res.* **2005**, *33*, No. e23.
(18) Leung, C.-H.; Chan, D. S.-H.; He, H.-Z.; Cheng, Z.; Yang, H.; Ma, D.-L. Luminescent Detection of DNA-Binding Proteins. *Nucleic Acids Res.* **2012**, *40*, 941−955.
(19) Xue, L.; Yu, Q.; Griss, R.; Schena, A.; Johnsson, K. Bioluminescent Antibodies for Point-of-Care Diagnostics. *Angew. Chem., Int. Ed.* **2017**, *56*, 7112−7116.
(20) Yu, Q.; Xue, L.; Hiblot, J.; Griss, R.; Fabritz, S.; Roux, C.; Binz, P.-A.; Haas, D.; Okun, J. G.; Johnsson, K. Semisynthetic Sensor Proteins Enable Metabolic Assays at the Point of Care. *Science* **2018**, *361*, 1122−1126.
(21) Zhang, Z.; Hejesen, C.; Kjelstrup, M. B.; Birkedal, V.; Gothelf, K. V. A DNA-Mediated Homogeneous Binding Assay for Proteins and Small Molecules. *J. Am. Chem. Soc.* **2014**, *136*, 11115−11120.
(22) Hansen-Bruhn, M.; Nielsen, L. D. F.; Gothelf, K. V. Rapid Detection of Drugs in Human Plasma Using a Small Molecule-Linked Hybridisation Chain Reaction. *ACS Sens.* **2018**, *3*, 1706−1711.
(23) Xu, L.; Zhang, H.; Yan, X.; Peng, H.; Wang, Z.; Zhang, Q.; Li, P.; Zhang, Z.; Le, X. C. Binding-Induced DNA Dissociation Assay for Small Molecules: Sensing Aflatoxin B1. *ACS Sens.* **2018**, *3*, 2590−2596.
(24) Rossetti, M.; Ippodrino, R.; Marini, B.; Palleschi, G.; Porchetta, A. Antibody-Mediated Small Molecule Detection Using Programmable DNA-Switches. *Anal. Chem.* **2018**, *90*, 8196−8201.
(25) Ranallo, S.; Rossetti, M.; Plaxco, K. W.; Vallée-Bélisle, A.; Ricci, F. A Modular, DNA-Based Beacon for Single-Step Fluorescence Detection of Antibodies and Other Proteins. *Angew. Chem., Int. Ed.* **2015**, *54*, 13214−13218.
(26) Jeong, H.-J.; Kojima, T.; Dong, J.; Ohashi, H.; Ueda, H. One-Pot Construction of Quenchbodies Using Antibody-Binding Proteins. *Anal. Methods* **2016**, *8*, 7774−7779.
(27) Abe, R.; Jeong, H.-J.; Arakawa, D.; Dong, J.; Ohashi, H.; Kaigome, R.; Saiki, F.; Yamane, K.; Takagi, H.; Ueda, H. Ultra Q-Bodies: Quench-Based Antibody Probes That Utilize Dye-Dye Interactions with Enhanced Antigen-Dependent Fluorescence. *Sci. Rep.* **2014**, *4*, 4640−4649.
(28) Hwang, H.; Myong, S. Protein Induced Fluorescence Enhancement (PIFE) for Probing Protein-Nucleic Acid Interactions. *Chem. Soc. Rev.* **2014**, *43*, 1221−1229.
(29) Valuchova, S.; Fulnecek, J.; Petrov, A. P.; Tripsianes, K.; Riha, K. A Rapid Method for Detecting Protein-Nucleic Acid Interactions by Protein Induced Fluorescence Enhancement. *Sci. Rep.* **2016**, *6*, 39653−39663.
(30) Stennett, E. M. S.; Ciuba, M. A.; Lin, S.; Levitus, M. Demystifying PIFE: The Photophysics behind the Protein-Induced Fluorescence Enhancement Phenomenon in Cy3. *J. Phys. Chem. Lett.* **2015**, *6*, 1819−1823.
(31) Kim, H.; Lee, C. Y.; Song, J.; Yoon, J.; Park, K. S.; Park, H. G. Protein-Induced Fluorescence Enhancement for a Simple and Universal Detection of Protein/Small Molecule Interactions. *RSC Adv.* **2018**, *8*, 39913−39917.
(32) Ploetz, E.; Lerner, E.; Husada, F.; Roelfs, M.; Chung, S.; Hohlbein, J.; Weiss, S.; Cordes, T. Förster Resonance Energy Transfer and Protein-Induced Fluorescence Enhancement as Synergetic Multi-Scale Molecular Rulers. *Sci. Rep.* **2016**, *6*, 33257.
(33) Rashid, F.; Raducanu, V.-S.; Zaher, M. S.; Tehseen, M.; Habuchi, S.; Hamdan, S. M. Initial State of DNA-Dye Complex Sets the Stage for Protein Induced Fluorescence Modulation. *Nat. Commun.* **2019**, *10*, 2104.
(34) Kjelstrup, M.; Nielsen, L.; Hansen-Bruhn, M.; Gothelf, K. A DNA-Based Assay for Digoxin Detection. *Biosensors* **2018**, *8*, 19−30.
(35) Carter, J. D.; LaBean, T. H. Coupling Strategies for the Synthesis of Peptide-Oligonucleotide Conjugates for Patterned Synthetic Biomineralization. *J. Nucleic Acids* **2011**, *2011*, 1−8.
(36) Bhuckory, S.; Lefebvre, O.; Qiu, X.; Wegner, K.; Hildebrandt, N. Evaluating Quantum Dot Performance in Homogeneous FRET Immunoassays for Prostate Specific Antigen. *Sensors* **2016**, *16*, 197−207.
(37) Gheorghiade, M.; Van Veldhuisen, D. J.; Colucci, W. S. Contemporary Use of Digoxin in the Management of Cardiovascular Disorders. *Circulation* **2006**, *113*, 2556−2564.
(38) Baldelli, S.; Cattaneo, D.; Pignatelli, P.; Perrone, V.; Pastori, D.; Radice, S.; Violi, F.; Clementi, E. Validation of an LC − MS / MS Method for the Simultaneous Quantification of Dabigatran , Rivaroxaban and Apixaban in Human Plasma. *Bioanalysis* **2016**, *8*, 275−283.
(39) Jung, M.; Rice, L. Treatment of Heparin-Induced Thrombocytopenia : What Are the Contributions of Clinical Trials. *Clin. Invest.* **2013**, *3*, 359−367.
(40) Stalker, D. J.; Jungbluth, G. L. Clinical Pharmacokinetics of Linezolid, a Novel Oxazolidinone Antibacterial. *Clin. Pharmacokinet.* **2003**, *42*, 1129−1140.
(41) Bezabeh, S.; Mackey, A. C.; Kluetz, P.; Jappar, D.; Korvick, J. Accumulating Evidence for a Drug−Drug Interaction Between Methotrexate and Proton Pump Inhibitors. *Oncologist* **2012**, *17*, 550−554.
(42) Husted, S.; De Caterina, R.; Andreotti, F.; Arnesen, H.; Bachmann, F.; Huber, K.; Jespersen, J.; Kristensen, S. D.; Lip, G. Y. H.; Morais, J.; Rasmussen, L. H.; Siegbahn, A.; Storey, R. F.; Weitz, J. I. Non-Vitamin K Antagonist Oral Anticoagulants (NOACs): No Longer New or Novel. *Thromb. Haemostasis* **2014**, *111*, 781−782.
(43) Gebhardt, C.; Lehmann, M.; Reif, M. M.; Zacharias, M.; Gemmecker, G.; Cordes, T. Molecular and Spectroscopic Characterization of Green and Red Cyanine Fluorophores from the Alexa Fluor and AF Series. *ChemPhysChem* **2021**, *22*, 1566−1583.
(44) Hawes, E. M.; Deal, A. M.; Funk-Adcock, D.; Gosselin, R.; Jeanneret, C.; Cook, A. M.; Taylor, J. M.; Whinna, H. C.; Winkler, A.

M.; Moll, S. Performance of Coagulation Tests in Patients on Therapeutic Doses of Dabigatran: A Cross-Sectional Pharmacodynamic Study Based on Peak and Trough Plasma Levels. *J. Thromb. Haemostasis* **2013**, *11*, 1493−1502.
(45) Burtis, C.; Ashwood, E.; Burns, D. *Tietz Textbook of Clinical Chemistry and Molecular Diagnostics*; Elsevier, 2005; p 2448.
(46) Richards, G. A.; Brink, A. J. Therapeutic Drug Monitoring: Linezolid Too? *Crit. Care* **2014**, *18*, 525−526.

https://doi.org/10.1021/acssensors.1c02642
ACS Sens. 2022, 7, 856−865